WILEY-VCH

DOI: 10.1002/((please add manuscript number))
Article type: Communication

Cobalt boride modified with N-doped carbon nanotubes as high-performance bifunctional oxygen electrocatalyst

Karina Elumeeva, Justus Masa, Danea Medina, Edgar Ventosa, Aziz Genç, Tim Bobrowski, Philipp Weide, Jordi Arbiol, Martin Muhler and Wolfgang Schuhmann**

Dr. K. Elumeeva, Dr. J. Masa, D. Medina, Dr. E. Ventosa, T. Bobrowski,
Prof. W. Schuhmann
Analytical Chemistry - Center for Electrochemical Sciences (CES)
Ruhr-Universität Bochum, Universitätsstr. 150, Bochum, D-44780 Germany
E-mail: justus.masa@rub.de, wolfgang.schuhmann@rub.de

A. Genç, Prof. J. Arbiol
Catalan Institute of Nanoscience and Nanotechnology (ICN2), CSIC and The Barcelona Institute of Science and Technology (BIST), Campus UAB, Bellaterra, 08193 Barcelona, Catalonia, Spain

Prof. J. Arbiol
ICREA, Pg. Lluís Companys 23, 08010 Barcelona, Catalonia, Spain

Dr. P. Weide, Prof. M. Muhler
Laboratory of Industrial Chemistry, Ruhr-Universität Bochum, Universitätsstr. 150, Bochum, D-44780 Germany

Keywords: oxygen evolution reaction; oxygen reduction reaction; bifunctional electrocatalyst; carbon nanotubes; cobalt boride; Zn-air batteries

Abstract

The development of reversible oxygen electrodes, able to drive both the oxygen evolution reaction (OER) and the oxygen reduction reaction (ORR) is still a great challenge. We describe a very efficient and stable bifunctional electrocatalytic system for reversible oxygen electrodes obtained by direct CVD growth of nitrogen-doped carbon nanotubes (NCNTs) on the surface of cobalt boride (CoB) nanoparticles. Detailed investigation of the crystalline structure and elemental distribution of CoB before and after NCNTs growth reveals that the NCNTs grow on small CoB nanoparticles formed in the CVD process. The resultant CoB/NCNT system exhibited outstanding activity in catalyzing both the OER and the ORR in

0.1 M KOH with an overvoltage difference of only 0.73 V between the ORR at -1 mA cm^{-2} and OER at +10 mA cm^{-2}. The proposed CoB/NCNT catalyst showed stable performance during 50 h of OER stability assessment in 0.1 M KOH. Moreover, CoB/NCNT spray-coated on a gas diffusion layer as an air-breathing electrode proved its high durability during 170 galvanostatic charge-discharge (OER/ORR) test cycles (around 30 h) at ±10 mA cm^{-2} in 6 M KOH, making it an excellent bifunctional catalyst for potential Zn-air battery application.

The growth of clean energy markets to mitigate effects of climate change and environmental pollution necessitates accelerated development of new systems able to store and convert renewable energy in the most efficient, nature-friendly and cost-effective ways. Rechargeable metal-air batteries have shown great promise to be used as future clean energy devices owing to their high energy densities and ability to use oxygen from the surrounding atmosphere as reactant.[1,2] Among the metal-air batteries, alkaline Zn-air batteries are the most intensively studied due to the abundance, stability in aqueous media, and high degree of safety of Zn in comparison to Li-air, Mg-air and Al-air battery systems, among others.[3,4] However, on the way to their widespread commercialization, it is important to not only solve problems related to corrosion and dendrite formation of the negative metal electrode but concomitantly to enhance the efficiency of the oxygen electrode. The efficiency of a rechargeable metal-air battery is limited by the reversibility of the oxygen electrode, which should efficiently drive both the oxygen reduction reaction (ORR) during the discharge cycle, and the oxygen evolution reaction (OER) during the charging cycle, both inherently sluggish reactions involving complex electrocatalysis.[5] Although many materials are reported to be impressive electrocatalysts for either the ORR or the OER,[6-9] with activities even exceeding the performance of noble-metal based electrocatalysts, a robust and durable bifunctional ORR/OER electrode able to reversibly catalyze both reactions over numerous charge-discharge cycles in highly concentrated alkaline solutions is yet to be developed.[3,10]

It has been demonstrated in various studies that nanocarbon materials doped with heteroatoms (N, S, P, B, F),[11-16] in most cases also incorporating non-precious transition metal species (Co, Fe, Mn, etc.),[17-20] efficiently reduce O_2 over a wide pH range. As concerns the OER, nowadays there are numerous active and stable non-precious catalysts that outperform precious-metal based catalysts.[7,21-23] The most common non-precious OER catalysts are based on oxides and hydroxides with one or several active metals and, sometimes, very sophisticated composition and structure.[24-27]

It is however still a great challenge to create a viable bifunctional porous electrode for reversible electrocatalysis of the OER and the ORR. One design strategy is to combine two efficient single-function catalysts for the individual reactions into a hybrid system by physical mixing [28], or to deploy two separate electrodes for the charge and discharge steps instead of a single bifunctional electrode.[21,29] A second possibility is to develop a single material, which can perform both functions, that is, efficiently catalyze the OER as well as the ORR.[30-32] For example, some complex oxides and hydroxides exhibit bifunctional activity for both ORR and OER.[33-35] Another approach is to introduce the second function to an efficient OER or ORR catalyst. This can be achieved, for instance, by the functionalization of OER-active perovskites with ORR active nitrogen-doped carbon functionalities and M-N_x/C moieties,[36] or by the calcination of metal salts in the presence of the ORR-active carbon nanomaterials to activate them for OER.[20,37] Bifunctional oxygen electrodes can also be obtained by CVD growth of carbon nanotubes (CNTs) on the surface of oxygen evolving catalysts such as spinels and perovskites.[38,39]

We report the successful transformation of cobalt boride (CoB), which was reported recently to possess exceptional OER activity at alkaline conditions,[22] into a highly efficient bifunctional OER/ORR electrocatalyst (CoB/NCNT) by direct CVD growth of NCNTs on the surface of CoB, where the CoB nanoparticles serve both as substrate and growth catalyst for the NCNTs. Noteworthy, the use of CoB as a catalyst for synthesis of carbon nanostructures

has hitherto not been reported. There was drastic improvement of the ORR activity achieved after growth of the NCNTs due to introduction of nitrogen-doped carbon functionalities, and a substantial gain in the OER activity ascribed to enhanced conductivity of the catalyst layer and higher dispersion of the CoB species after the CVD process. CoB/NCNT demonstrated excellent performance as a bifunctional ORR/OER catalyst, the voltage difference between the ORR at -1.0 mA cm^{-2} and the OER at 10 mA cm^{-2} in 0.1 M KOH being as low as 0.73 V. In addition, the catalyst demonstrated outstanding durability after 170 charge-discharge cycles at a current density of ±10 mA cm^{-2} in 6 M KOH under practical Zn-air battery conditions.

We envisioned that modifying amorphous cobalt boride (CoB), which was recently reported to be a very efficient catalyst for OER,[22] with nitrogen-doped carbon nanotubes (NCNTs) would not only improve the OER activity of the catalyst due to conductivity enhancement but also introduce active sites exhibiting oxygen reduction functionality thus yielding a highly active ORR/OER bifunctional catalyst. To achieve reasonable OER activity enhancement, it is vital to establish intimate contact between the CoB nanoparticle and the NCNTs, which cannot be realized by simple mixing of pre-synthesized NCNTs with CoB. In this work, NCNTs were hence directly grown on the surface of CoB nanoparticle by the CVD method at relatively low temperatures, and a low ethylene concentration in the supporting gas as carbon source to control the rate of growth of the NCNTs and their coverage over the CoB nanoparticles. From the SEM images shown in **Figure 1**, it is clear to note that the morphology of the carbon deposits on the CoB nanoparticles was strongly dependent on the synthesis temperature. Higher temperatures yielded longer and thicker carbon nanotubes. At 500 °C, relatively thinner and shorter carbon nanotubes with average diameter from 20 to 25 nm densely cover the surface of the CoB nanoparticles. At 600 and 700 °C, the average diameter of the tubes was between 35-45 nm, however, much thicker tubes or filaments with diameters larger than 80 nm are also visible. The observed difference in the CNT diameter

and length can be explained by faster ethylene decomposition at higher temperatures, sintering of CoB particles, and faster carbon diffusion over the active CoB nanoparticles leading to formation of larger carbon nuclei.[40] However, temperature was not the only parameter which strongly influenced the nucleation and growth of the CNTs. Variation of the catalyst composition, which influences the metal-carbon (M-C) bond strength, the nature of the carbon carrier including its concentration in the flow stream and its flow rate, as well as duration of the synthesis can lead to CNTs of diverse morphologies.[40-42] In this work, we exclusively focused on the influence of temperature on the properties of the CNTs, and on the electrochemical performance of the resulting CoB/NCNT catalysts.

Doping of the CNTs with nitrogen was achieved by including NH_3 in the ethylene gas stream during their growth. Elemental analysis revealed the presence of nitrogen in the CoB/NCNT bifunctional catalysts (**Table 1**). The carbon content increased with the synthesis temperature, with the most drastic increase occurring for the increase from 500 to 600 °C. However, the nitrogen content decreased with the temperature possibly due to formation of volatile C-N compounds and faster decomposition of ammonia at higher temperatures.

High resolution transmission electron microscopy (HRTEM) and scanning TEM (STEM) combined with electron energy loss spectroscopy (EELS), in the respective order, were used to analyze the microstructure of the initial CoB catalyst and the CoB/NCNT system, and the distribution of the constituent elements within the samples. The initial CoB sample which is an active catalyst for water splitting[22] possesses a flake-like structure (**Figure S1a**). The HRTEM micrograph in **Figure S1b** of a large agglomerate revealed nanocrystallinity of the initial sample. Fast Fourier-transform (FFT) patterns (power spectra) of selected areas show that the nanocrystallites exhibit a simple orthorhombic phase (space group: Pbnm) with lattice parameters of a = 0.3984 nm, b = 0.5243 nm and c = 0.3307 nm, when visualized along the [100] zone axis, which is indexed to crystalline CoB. Local elemental quantification by

EELS (**Figure S3c**) showed the atomic ratio of Co:B to be close to 1:1, which further supports the existence of cobalt boride as CoB. However, the existence of the particles in other crystalline forms of cobalt boride, such as Co_2B and Co_3B, cannot be excluded. It should be noted that the crystalline structure of this type of compounds is very sensitive to the post synthesis thermal treatment temperature.[22] EELS elemental composition maps of Co (red), B (green), O (blue) and C (turquoise) along with those of the Co – B and Co – O composites are presented in **Figure S3c**. The EELS elemental maps show that Co and B were homogeneously distributed throughout the mapped region with the exception of the peripheral areas that seem to contain relatively less boron. This is attributed to surface oxidation since Co and O intensities are relatively higher at the peripheral domains. The presence of C is rather weak in CoB, and arises from the residual organic solvents used in the preparation.

The annular dark field (ADF) STEM image in **Figure 2a** shows that after CVD growth of the NCNTs, the thin cobalt boride sheets were transformed into small spherical nanoparticles distributed within the carbon nanotube matrix. Most of the CoB nanoparticles are on the surface of the carbon nanotubes, while some are encapsulated inside of the tube core as depicted in **Figures 2b,c,e**. The small nanoparticles formed during the CVD process due to the reductive atmosphere evidently act as nuclei for the NCNTs growth.

The NCNTs consisted of stacks of graphitic layers as can be seen in **Figures 2c,d**. For the analyzed sample (CoB/NCNT-500), we attribute the formation of this kind of structure to the rather low synthesis temperature and to the unusual composition of the CNT growth catalyst particles.

The HRTEM images presented in **Figure 2b,c,e** reveal conically shaped particles embedded inside the CNTs, which evidently participated in the growth of the CNTs. The conical shape arises due to the strong capillary forces inside the tubes during their growth. The power spectrum of an encapsulated particle (**Figure 2e**), visualized along its [011] zone axis, revealed that this nanoparticle is composed of the same orthorhombic CoB phase.

Several conclusions can be drawn from the EELS elemental composition maps of a single nanotube with a nanoparticle at one of its ends (**Figure 2f**). The maps show the distribution of Co (red), B (green), O (blue), C (turquoise) and N (violet). One can observe that: *(i)* Co and B are homogeneously distributed within the nanoparticle, *(ii)* the surface of the nanoparticles is oxidized, and *(iii)* the CNTs contain a substantial amount of N. Since metal borides, in this specific case, cobalt boride, has to the best of our knowledge, never been reported as a growth catalyst for CNTs, this is the first explicit observation of a metal boride acting as catalyst for CNT growth. We therefore suppose that the presence of boron inside active catalytic nanoparticles for CNT growth could strongly influence the morphology and properties of the CNTs.

Analysis of the elemental distribution in the ensemble of nanoparticles and nanotubes presented in **Figure S2** reveals that cobalt and boron are homogeneously distributed within the particles, with the particle surfaces being partially oxidized. Moreover, the carbon deposits contain a substantial amount of nitrogen within their structure (as shown in **Figure 2f**), which should certainly promote the ORR activity of the samples.

XPS studies on the chemical state of the catalyst surfaces (before and after NCNT growth) confirmed the presence of Co, O, N, C and B as expected from the synthesis conditions. The high-resolution B 1s spectra of all samples have a wide signal in the 189-192 eV binding energy range whose intensity decreased with increasing synthesis temperature. This is expected to be due to higher coverage of the cobalt boride particles with NCNTs, thus decreasing their surface availability for detection by XPS (**Figure 3a**). The B 1s spectrum is dominated by boron oxo-species, which is typical of amorphous metal-borides exposed to atmospheric conditions.[22] High-resolution N 1s spectra show that all the samples contain contributions of pyridinic nitrogen at around 398.5 eV, graphitic nitrogen in the range of 399.9-401 eV, and a weak signal of oxidized nitrogen in the range of 402-405 eV.[14,43] It was observed, though, that the sample prepared at 700 °C has a relatively higher intensity of

quaternary nitrogen species presumably due to the formation of carbon nanotubes with extended graphitic walls where nitrogen atoms are embedded in the graphitic structure. The Co 2p region (**Figure 3c**) shows two sets of broad peaks, around 778-781.7 eV and 795.1-796.0 eV corresponding to the $2p_{3/2}$ and $2p_{1/2}$ core levels, respectively.[44,45] Deconvolution of the Co $2p_{3/2}$ region revealed two main species, Co-B in crystalline cobalt boride at around 778.5 eV, and Co^{2+} at about 781.0 eV due to surface-oxidized cobalt, consistent with literature reports on cobalt boride.[22,44]

The bifunctional electrocatalytic activity of the CoB/NCNT catalysts prepared at different temperatures was first investigated in a 3-electrode electrochemical cell in oxygen-saturated 0.1 M KOH. Linear sweep voltammograms (LSV) of the catalyst recorded at a scan rate of 5 mV s^{-1} and electrode rotation speed of 1600 rpm are presented in **Figure 4a**. All the CoB/NCNT-***x*** samples showed very good activity in catalyzing both the ORR and the OER. However, the most active sample with the lowest overpotentials for both reactions was CoB/NCNT-500. Most importantly, the voltage difference between the ORR at -1 mA cm^{-2} and the OER at +10 mA cm^{-2} for this catalyst was found to be only 0.73 V (**Table 2**), which is much lower than benchmark values for the majority of non-precious bifunctional ORR/OER electrocatalysts reported to date.[46]

Temperature increase above 500 ^{o}C resulted in a dramatic drop of the OER activity, which can be explained by the formation of thicker and longer carbon nanotubes over the surface of cobalt boride particles, potentially inhibiting accessibility of the reactant (water) to the active sites. Thus, the excellent bifunctional activity of CoB/NCNT-500 is attributed to optimal coverage with much shorter NCNTs. The drastic structural change of cobalt boride after growth of the NCNTs, as observed by HRTEM, did not affect its OER activity probably due to sufficient abundance of accessible CoB species not blocked by the NCNTs serving as the main OER active domains. Instead, we observed slight improvement of OER activity, mainly ascribed to enhanced conductivity of the catalytic layer and due to a more favorable

distribution of the active sites. Moreover, the oxygen reduction activity improved substantially after NCNT growth in comparison to the initial ORR activity of CoB. It is supposed that the main active species for the ORR resided on the surface of the NCNTs. However, the small cobalt boride nanoparticles distributed within the NCNT matrix can complement ORR electrocatalysis by serving as active species, as demonstrated in **Figure 4a**, or by promoting the ORR reaction through secondary effects such as modulating the chemisorption energy of molecular oxygen and the intermediates involved in the ORR. Interestingly, the presence of boron within a carbon matrix can also play a major role in enhancing the ORR activity of the CoB/NCNT catalysts.[11]

The other important parameter of bifunctional catalysts that has to be evaluated is the selectivity of the ORR. The yield of H_2O_2 generated during the ORR was evaluated by RRDE experiments (**Figure 4b-d**) and found to be very low (less than 3%) for CoB/NCNT-500, the best sample. From the RRDE data, **Figure 4d**, it is clear to see that oxygen was mostly reduced directly to water via the 4-electron pathway, which is desirable since it facilitates a higher discharge current, moreover, the production of H_2O_2, a destructive by-product to cell components, is minimized.

We investigated the OER stability of CoB/NCNT-500 to assess its stability under the highly oxidative OER conditions. Preliminary stability tests performed in a 3-electrode flow-through cell exhibited a barely noticeable potential increase after 51 h of continuous galvanostatic OER polarization at +10.2 mA cm^{-2} indicating electrocatalytic stability of the CoB/NCNT-500 catalyst for the OER (**Figure 4e**). After this test, the catalyst film was collected and investigated by STEM-EELS analysis (**Figure S3**). Elemental distribution maps of the electrochemically activated catalyst revealed the presence of boron inside the catalyst particles. This suggests that boron remains a part of the active catalyst during the OER.

A bifunctional electrocatalyst for e.g. rechargeable alkaline Zn-air batteries should not only be stable under the harsh conditions of the OER, but should also retain its activity when

repeatedly switched from OER to ORR conditions and vice versa. Consequently, the stability of CoB/NCNT-500 immobilized on a gas diffusion layer of an air-breathing electrode upon charge-discharge (ORR/OER) cycling at a current density of ±10 mA cm^{-2} and at the KOH concentration used in Zn-air batteries (6 M) was evaluated in a 3-electrode cell (**Figure S4**). The evolution of the potential of the air-breathing electrode during the first two cycles is shown in **Figure 5a**. The overpotential difference between the OER and ORR for the first cycle was only 0.855 V, which is an excellent value especially at the comparatively high current density of ±10 mA cm^{-2} especially with respect to the ORR. The potential for the OER did not change from the first to the second cycle while that for the ORR decreased by 0.05 V. This indicates that the ORR activity of CoB/NCNT-500 declined after subjecting it to the anodic OER conditions. After the second ORR/OER cycle, the potential for both the OER and ORR remained constant during the rest of the stability test (**Figure 5b**) showing a constant voltage difference between the OER and ORR of 0.860 V for at least 170 cycles (30 h). This demonstrates that CoB/NCNT-500 does not only possess excellent activity and selectivity as a bifunctional electrocatalyst, but also very high stability as a reversible air-electrode for potential applications in rechargeable Zn-air batteries.

In summary, we have developed a novel highly efficient bifunctional electrocatalyst with excellent activity for oxygen evolution and reduction by direct growth of nitrogen-doped carbon nanotubes (NCNTs) on cobalt boride (CoB) particles. Importantly, the possibility of using cobalt boride as a catalyst for CNT growth as confirmed by detailed structure and composition studies was demonstrated for the first time. CoB/NCNT-500 exhibited excellent activity as a bifunctional catalyst displaying a voltage difference between the OER (+10 mA cm^{-2}) and ORR (-1 mA cm^{-2}) of only 0.73 V. Additionally, the catalyst was found to reduce oxygen selectively to water via the 4-electron transfer pathway. Post mortem analysis of the electrochemically activated CoB/NCNT-500 catalyst subjected to OER conditions revealed

surface oxidation of CoB, forming a core-shell (CoO_x-CoB) structure. Moreover, air-breathing electrodes composed of CoB/NCNT spray-coated onto a gas diffusion layer exhibited outstanding stability upon numerous galvanostatic charge-discharge (ORR-OER) cycles at ±10 mA cm^{-2} in 6 M KOH for at least 30 h (170 ORR/OER cycles), thus demonstrating its potential applicability for rechargeable Zn-air battery technology.

Experimental Section

Preparation of bifunctional CoB/NCNT electrocatalysts: Cobalt boride (denoted here as CoB for simplicity) nanoparticles later used as substrate and catalyst for NCNT growth were synthesized by reaction of $CoCl_2$ with $NaBH_4$ under argon atmosphere according to the procedure described previously.[22] The formed black precipitate was washed, first with ultrapure water then with ethanol and vacuum dried. Carbon nanostructures were grown on the surface of the CoB nanoparticles by chemical vapor deposition (CVD). To perform the CVD synthesis, 100 mg of the CoB powder were placed in a quartz boat and inserted in the center of a tubular 3-zone furnace. Pure N_2 was first flushed into the reactor for 15 min, then the temperature was ramped at 10 °C min^{-1} under continuous nitrogen flow (100 ml min^{-1}) until the CNT synthesis temperature (500-700 °C) was reached. At this temperature, a C_2H_4/NH_3/He mixture in a 5:10:85 volume ratio and at a flow rate of 100 ml min^{-1} was passed through the reactor for 5 h. After this, the reactor was cooled down to room temperature under nitrogen atmosphere. The obtained catalysts, denoted as CoB/NCNT-***x***, where ***x*** is the synthesis temperature (500-700 °C), were used for physico-chemical and electrochemical characterization without any further treatment.

Structural characterization: Scanning electron microscopy (SEM) images were obtained using a Quanta 3D FEG scanning electron microscope (FEI) operated at 20.0 kV. Elemental analysis was performed using a VarioEL III analyzer (Elementar Analysensysteme) to deter-

mine the concentration of C, N and H. TEM studies were conducted using a field emission gun FEI Tecnai F20 microscope operated at 200 kV, equipped with a high angle annular dark field (HAADF) detector and a Quantum Gatan Image Filter (GIF) for electron energy-loss spectroscopy (EELS) analyses. X-ray photoelectron spectroscopy (XPS) measurements were carried out in an ultra-high vacuum (UHV) set-up equipped with a monochromatic Al Kα X-ray source (1486.6 eV; anode operating at 14 kV and 30.5 mA) and a high-resolution Gammadata-Scienta SES 2002 analyzer. The base pressure in the measurement chamber was maintained at about 7×10^{-10} mbar. A flood gun was applied to compensate for the charging effects. The binding energies were calibrated based on the C 1s peak at 284.8 eV. The CasaXPS program with a Gaussian-Lorentzian mixed function and Shirley background subtraction was used to analyze the spectra.

Standard electrochemical measurements in 0.1 M KOH solution: Catalyst inks were prepared by dispersion of 5 mg of the catalyst powder in 1 ml of a solution containing ultra-pure water, ethanol and Nafion solution (5 wt. %) in a volume ratio of 49:49:2 with the aid of ultrasonication for at least 20 min to ensure formation of a homogeneous suspension. Glassy carbon rotating disk electrodes (RDE) and rotating ring-disk electrodes (RRDE) of 4 mm and 5.6 mm diameter, respectively, modified with the catalyst film were used as working electrodes, while a Ag/AgCl/3 M KCl and a platinum mesh were used as reference and counter electrode, respectively. Prior to modification with the catalyst film, the electrodes were polished with 1 µm and 0.3 µm alumina pastes, and rinsed with water. Afterwards, 5.3 µL and 10.6 µL of catalyst ink were drop-cast onto the RDE and RRDE surfaces, respectively, and air dried to obtain a catalyst film with a nominal catalyst loading of 210 µg cm^{-2}. Preliminary electrocatalytic measurements were carried out at room temperature in a coaxial three-electrode cell containing oxygen saturated 0.1 M KOH, using a Metrohm potentiostat/galvanostat (AutolabIII/FRA2) with a RDE 710 rotator (Gamry Instruments). To correct the electrochemical data for the uncompensated solution resistance (iR drop), electrochemical impedance spectroscopy (EIS)

measurements were conducted before each experiment at open circuit potential (OCP). The AC perturbation voltage was 10 mV_{pp} in the frequency range between 10 kHz and 200 Hz. The electrolyte resistance was obtained from the intercept of the Nyquist plot at high frequencies on the real impedance axis. Before acquiring any electrochemical data, a conditioning step was applied by continuous potential cycling between 0.1 and -0.5 V vs. Ag/AgCl/3 M KCl at a scan rate of 100 mV s^{-1} until reproducible cyclic voltammograms (CVs) were obtained. Finally, linear sweep voltammograms (LSV) were recorded at a scan rate of 5 mV s^{-1} and at 1600 rpm electrode rotation, first in the potential range from 0.1 to -1.0 V for ORR, and then from 0.1 V to +1.0 V for OER. The ORR tests were performed prior to the OER tests to avoid the influence of bubble formation during the OER on the reliability of the ORR measurements. All potentials were converted to the reversible hydrogen electrode scale (RHE) according to the equation:

$$E_{RHE} = E_{Ag/AgCl} + 0.059\,pH + E^{o}{}_{Ag/AgCl}$$

The pH value was calculated using the equation: pH = 14 + log [OH^-] + logγ, where the OH^- concentration was corrected using the KOH purity (85 %) and the activity coefficient of a 0.1 M KOH γ = 0.766 was taken from reference [47].

The selectivity of the catalyst during ORR was evaluated by RRDE voltammetry measurements, in which the ring potential was set to 1.3 V vs RHE meanwhile the disk potential was scanned from 0.1 V to -1.0 V at a rotation speed of 1600 rpm. The yield of H_2O_2, and the number of transferred electrons (n) were calculated from the RRDE data according to the following equations:

$$H_2O_2(\%) = 200 \times \frac{I_R/N}{I_R/N + I_D} \qquad n = 4 \times \frac{I_D}{I_R/N + I_D}$$

I_D and I_R are the disk and ring currents, respectively, and N is the collection efficiency determined for each modified catalyst film in 0.1 M KOH solution containing 5 mM potassium ferrocyanide at 1600 rpm.[48]

Long-term durability tests of the bifunctional catalysts were conducted by galvanostatic measurements in a specifically designed flow-through, three-electrode electrochemical cell.[49] The electrocatalyst films were prepared in the same way as for RDE and RRDE experiments; however, the catalyst loading was increased to 300 µg cm^{-2} in order to obtain homogeneous films on the surface of a graphite foil electrode. A Pt mesh was used as counter electrode and a Ag/AgCl/3 M KCl as reference electrode. In this cell geometry, 0.1 M KOH pre-saturated with oxygen was continuously pumped through the cell at a flow rate of 25 mL min^{-1}. OER stability tests were evaluated by galvanostatic polarization at a fixed current of 2 mA (around 10.2 mA cm^{-2}) for 50 h. The stability test involved a repeating sequence of galvanostatic polarization for 0.5 h with intermediary stabilization and EIS measurements used for iR correction. After the stability test, the catalyst film was carefully removed from the electrode surface and analyzed by (S)TEM and EELS.

Battery tests in a 3-electrode configuration: To evaluate the practicality of the CoB/NCNT bifunctional catalyst for rechargeable zinc-air battery applications, its activity and stability were further evaluated in a home-built electrochemical cell shown in **Figure S4**. The air-electrode was prepared by spray-coating a suspension of the catalyst onto a commercially available carbon cloth gas diffusion layer (MTI) to a loading of about 1.0 mg cm^{-2} (based on the geometric surface area). The performance of spray-coated electrodes was compared to that of drop-coated samples and has shown improved bifunctional activity due to a more homogeneous particle distribution (**Figure S5**). The catalyst loading was calculated by weighting the electrode before and after spray-coating. The catalyst ink was prepared by dispersing 8.0 mg of the catalyst powder and 32 µL of Nafion (5 wt. %) in 8 mL of ethanol followed by

sonication for 30 min. The electrolyte used was 6 M KOH. $Ni(OH)_2$ was used as counter electrode to ensure that *i)* side products (e.g. H_2) that might affect the measurement at the air-electrode are not produced at the counter electrode and *ii)* the stability measurement is not limited by cyclability of the counter electrode. A commercial Hg/Hg_2Cl_2 (KCl sat) electrode was used as the reference electrode. The potentials are given against $Zn/Zn(OH)_4^{2-}$ (6 M KOH) to facilitate interpretation of the air-electrode performance. Galvanostatic charge-discharge (OER-ORR) cycling measurements were carried out at a current density of ±10 mA cm^{-2}, lasting 10 min for each half-cycle. During the measurements, oxygen was continuously introduced to maintain oxygen saturation in the electrolyte.

Supporting information

Supporting Information is available from the Wiley Online Library or from the author.

Acknowledgements

The authors are grateful to the Deutsche Forschungsgemeinschaft (DFG) in the framework of the Cluster of Excellence "RESOLV" (EXC1069) and the Bundesministerium für Bildung und Forschung (BMBF) in the framework of the project "Mangan" (FKZ 03EK3548). J.A. and A.G. acknowledge the funding from the Generalitat de Catalunya 2014SGR1638. A.G. and J.A. acknowledge funding from Spanish MINECO e-TNT (MAT2014-59961-C2-2-R) project. ICN2 acknowledges support from the Severo Ochoa Program (MINECO, Grant SEV-2013-0295).

Received:
Revised:
Published online:

References

[1] X. Zhang, X.-G. Wang, Z. Xie, Z. Zhou, *Green Energy Environ.* **2016**, *1*, 4.

[2] Y. Li, H. Dai, *Chem. Soc. Rev.* **2014**, *43*, 5257.

[3] V. Caramia, B. Bozzini, *Mater. Renew. Sustain. Energy* **2014**, *3*, 28.

[4] F. Cheng, J. Chen, *Chem. Soc. Rev.* **2012**, *41*, 2172

[5] T. Shinagawa, A.T. Garcia-Esparza, K. Takanabe, *Sci. Rep.* **2015**, *5*, 1.

[6] Y. Cheng, S. P. Jiang, *Prog. Nat. Sci.* **2015**, *25*, 545.

[7] E. Fabbri, A. Habereder, K. Waltar, R. Kötz, T. J. Schmidt, *Catal. Sci. Technol.* **2014**, *4*, 3800.

[8] M. Shao, Q. Chang, J. P. Dodelet, R. Chenitz, *Chem. Rev.* **2016**, *116* (6), 3594.

[9] F. Jaouen, E. Proietti, M. Lefevre, R. Chenitz, J.-P. Dodelet, G. Wu, H.T. Chung, C. M. Johnston, P. Zelenay, *Energy Environ. Sci.* **2011**, *4*, 114.

[10] A. R. Mainar, O. Leonet, M. Bengoechea, I. Boyano, I. de Meatza, A. Kvasha, A. Guerfi, J. A. Blázquez, *Int. J. Energy Res.* **2016**, *40*, 1032.

[11] C. H. Choi, S. H. Park, S. I. Woo, *ACS Nano* **2012**, *6(8)*, 7084.

[12] K. Gong, F. Du, Z. Xia, M. Durstock, L. Dai, *Science* **2009**, *323*, 760.

[13] S. Chen, J. Bi, Y. Zhao, L. Yang, C. Zhang, Y. Ma, Q. Wu, X. Wang and Z. Hu, *Adv. Mater.* **2012**, *24*, 5593.

[14] K. Elumeeva, N. Fechler, T.P. Fellinger, M. Antonietti, *Mater. Horizons* **2014**, *1*, 588.

[15] Y. Zheng, Y. Jiao, L. Ge, M. Jaroniec and S. Z. Qiao, *Angew. Chem., Int. Ed.* **2013**, *52*, 3110.

[16] J. Masa, A. Zhao, W. Xia, M. Muhler, W. Schuhmann, *Electrochim. Acta* **2014**, *128*, 271.

[17] G. Wu, K. L. More, C. M. Johnston, P. Zelenay, *Science* **2011**, *332*, 443.

[18] K. Elumeeva, J. Ren, M. Antonietti, T.-P. Fellinger, *ChemElectroChem*. **2015**, *2*, 584.

[19] J. Masa, W. Xia, M. Muhler, W. Schuhmann, *Angew. Chem. Int. Ed.* **2015,** *54*, 10102.

[20] Z. Wang, S. Xiao, Z. Zhu, X. Long, X. Zheng, X. Lu, S. Yang, *ACS Appl. Mater. Interf.* **2015**, *7*, 4048.

[21] M. Gong, H. Dai, *H. Nano Res.* **2015**, *8*, 23.

[22] J. Masa, P. Weide, D. Peeters, I. Sinev, W. Xia, Z. Sun, C. Somsen, M. Muhler, W. Schuhmann, *Adv. Energy Mater.* **2016,** *6*, 1502313.

[23] J. Masa, S. Barwe, C.Andronescu, I. Sinev, A. Ruff, K. Jayaramulu, K. Elumeeva, B. Konkena, B. R.Cuenya,W. Schuhmann, *ACS Energy Lett.* **2016**, *1 (6)*, 1192.

[24] C. C. L. McCrory, S. Jung, J. C. Peters, T. F. Jaramillo, *J. Am. Chem. Soc.* **2013**, *135*, 16977.

[25] M. S. Burke, L. J. Enman, A. S. Batchellor, S. Zou, S. W. Boettcher, *Chem. Mater.* **2015**, *27*, 7549.

[26] X. Long, Z. Wang, S. Xiao, Y. An, S. Yang, *Mater. Today*. **2016**, *19*, 213

[27] F. Dionigi, P. Strasser, *Adv. Energy Mater.* **2016**, *6*, 1600621.

[28] K. Elumeeva, J. Masa, F. Tietz, F. Yang, W. Xia, M. Muhler, W. Schuhmann, *ChemElectroChem*. **2016**, *3*, 138.

[29] Y. G. Li, M. Gong, Y. Y. Liang, J. Feng, J. E. Kim, H. L. Wang, G. S. Hong, B. Zhang, H. J. Dai, *Nat. Commun.* **2013**, *4*, 1805.

[30] A. Zhao, J. Masa, W. Xia, A. Maljusch, M. Willinger, G. Clavel, K. Xie, R. Schlögl, W. Schuhmann M. Muhler, *J. Am. Chem. Soc.* **2014**, *136*, 7551.

[31] B. Y. Xia, Y. Yan, N. Li, H. B. Wu, X. W. Lou, X. Wang, *Nat. Energy* **2016**, *1*, 1.

[32] S. Gadipelli, T. Zhao, S. A. Shevlin, Z. Guo, *Energy Environ. Sci*. **2016**, *9*, 1661.

[33] Y. Gorlin, T. F. Jaramillo, *J. Am. Chem. Soc.* **2010**, *132*, 13612.

[34] J.-I. Jung, M. Risch, S.Park, M. G. Kim, G. Nam,H.-Y. Jeong, Y.Shao-Horn, J. Cho, *Energy Environ. Sci.* **2016**, *9*, 176.

[35] S. Gupta, W. Kellogg, H. Xu, X. Liu, J. Cho, G. Wu, *Chem. Asian J.* **2016**, *11*, 10.

[36] R. A. Rincón, J. Masa, S. Mehrpour, F. Tietz, W. Schuhmann, *Chem. Comm.* **2014**, *50*, 14760.

[37] X. Liu, M. Park, M. G. Kim, S. Gupta, X. Wang, G.Wu, J. Cho, *Nano Energy* **2016**, *20*, 315.

[38] K. Elumeeva, J. Masa, J. Sierau, F. Tietz, M. Muhler, W. Schuhmann, *Electrochim. Acta* **2016**, *208*, 25.

[39] Z. Chen, A. Yu, D. Higgins, H. Li, H. Wang, Z. Chen, *Nano Lett.* **2012**, *12*, 1946.

[40] J.-P. Tessonnier, D.S. Su, *ChemSusChem*. **2011**, *4*, 824.

[41] V.L. Kuznetsov, D.V. Krasnikov, A.N. Schmakov, K.V. Elumeeva, *Physica Status Solidi B* **2012**, *249*, 2390.

[42] V. L. Kuznetsov, A. N. Usoltseva, A. L. Chuvilin, E. D. Obraztsova, J. M. Bonard, *Phys. Rev. B.* **2001**, *64*, 235401.

[43] J. P. Paraknowitsch, J. Zhang, D. Su, A. Thomas, M. Antonietti, *Adv. Mater.* **2010**, *22*, 87.

[44] S. Gupta, N. Patel, A. Miotello, D. C. Kothari, *J. Power Sources* **2015**, *279*, 620.

[45] S. Cobo, J. Heidkamp, P.A. Jacques, J. Fize, V. Fourmond, L. Guetaz, B. Jousselme, V. Ivanova, H. Dau, S. Palacin, M. Fontecave, V. Artero, *Nat. Mater.* **2012**, *11*, 802.

[46] M. Wang, T. Qian, J. Zhou, C. Yan, *ACS Appl. Mater. Interfaces* **2017**, *9*, 5213.

[47] M. Knobel, J. Am. Chem. Soc. **1923**, *45*, 70

[48] U.A. Paulus, T.J. Schmidt, H.A. Gasteiger, R.J. Behm, *J. Electroanal. Chem.* **2001**, *495*, 134.

[49] A. Maljusch, O. Conradi, S. Hoch, M. Blug, W. Schuhmann, *Anal. Chem.* **2016**, *88*, 7597.

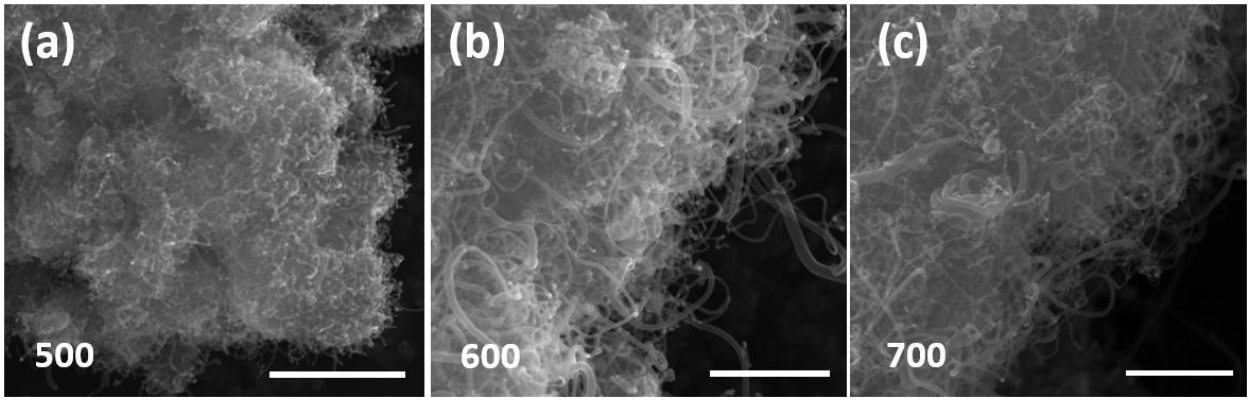

Figure 1. SEM images of CoB/NCNT bifunctional electrocatalysts prepared at different temperatures: a) 500º C. b) 600º C. c) 700º C. Scale bar 1 µm.

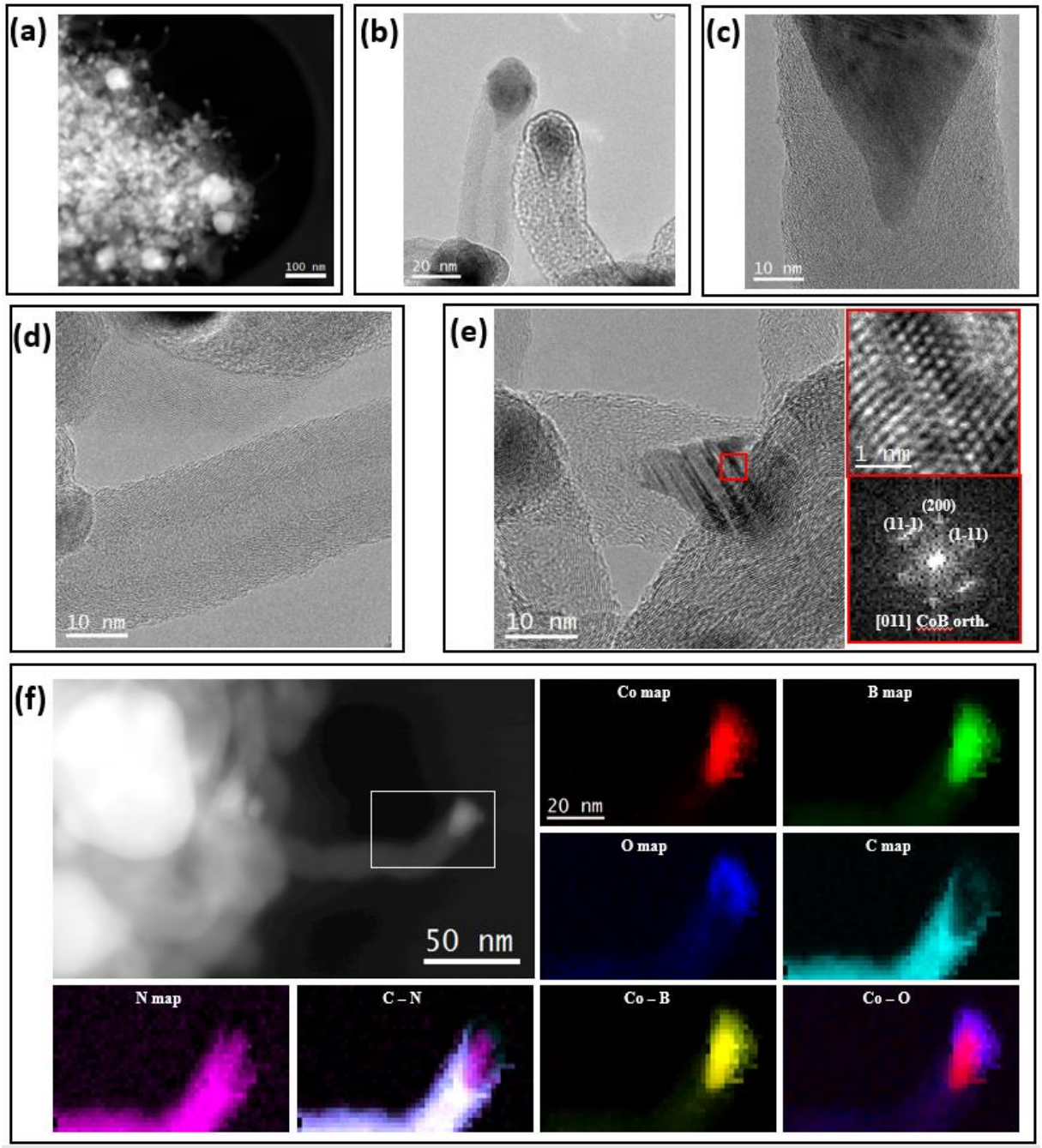

Figure 2. (S)TEM analysis of the CoB/NCNT-500 sample before the electrochemical test: a) ADF STEM micrograph. b-e) High-resolution TEM images of individual CNTs and encapsulated CoB nanoparticles, and detailed microstructure of the red squared region (e) and its corresponding power spectrum. f) ADF STEM micrograph of the ensemble of nanoparticles and nanotubes and STEM – EELS elemental composition maps of the area indicated with a white rectangle: Co (red), B (green), O (blue), C (turquoise) and N (violet) and their overlay (Co – B, Co – O and C – N). The scale bar is the same for all the compositional maps.

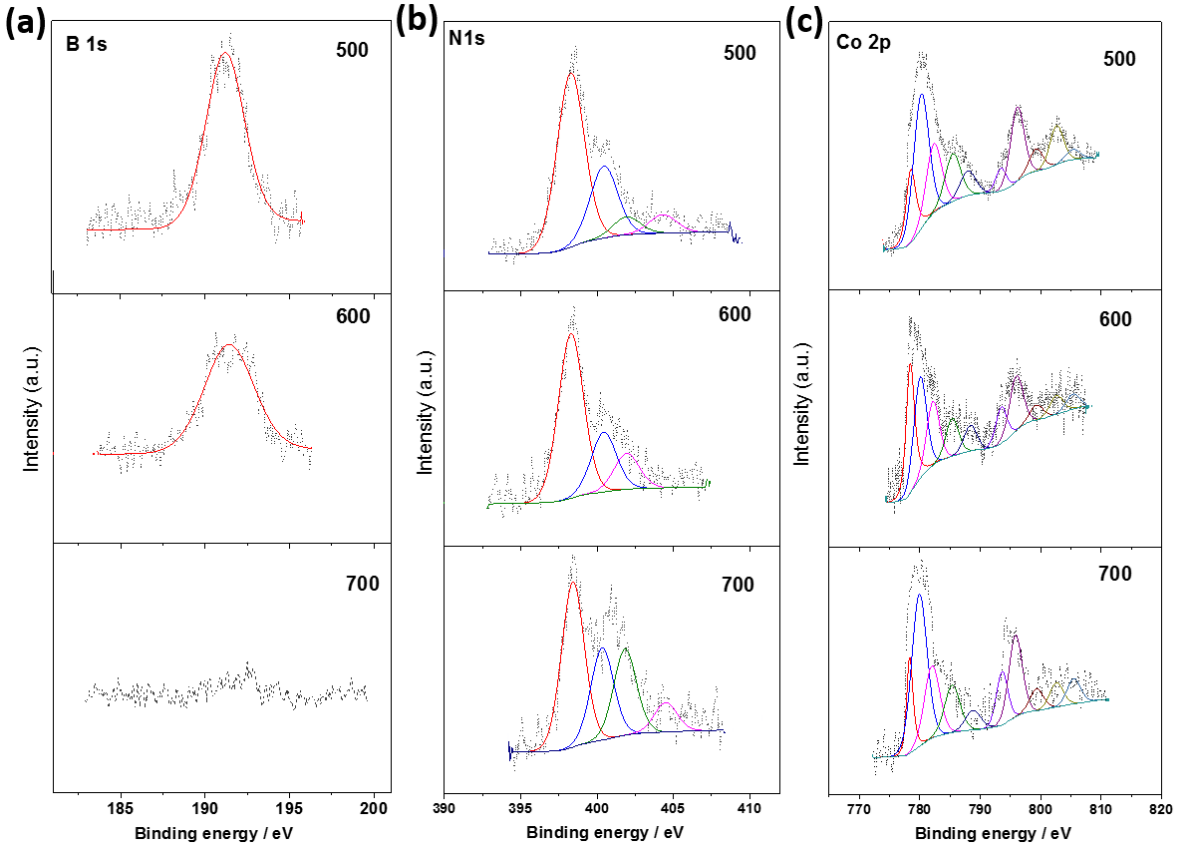

Figure 3. a-c) XPS characterization of CoB/NCNT catalysts prepared at 500, 600 and 700 °C: B 1s (a), N 1s (b), Co 2p (c) core levels spectra.

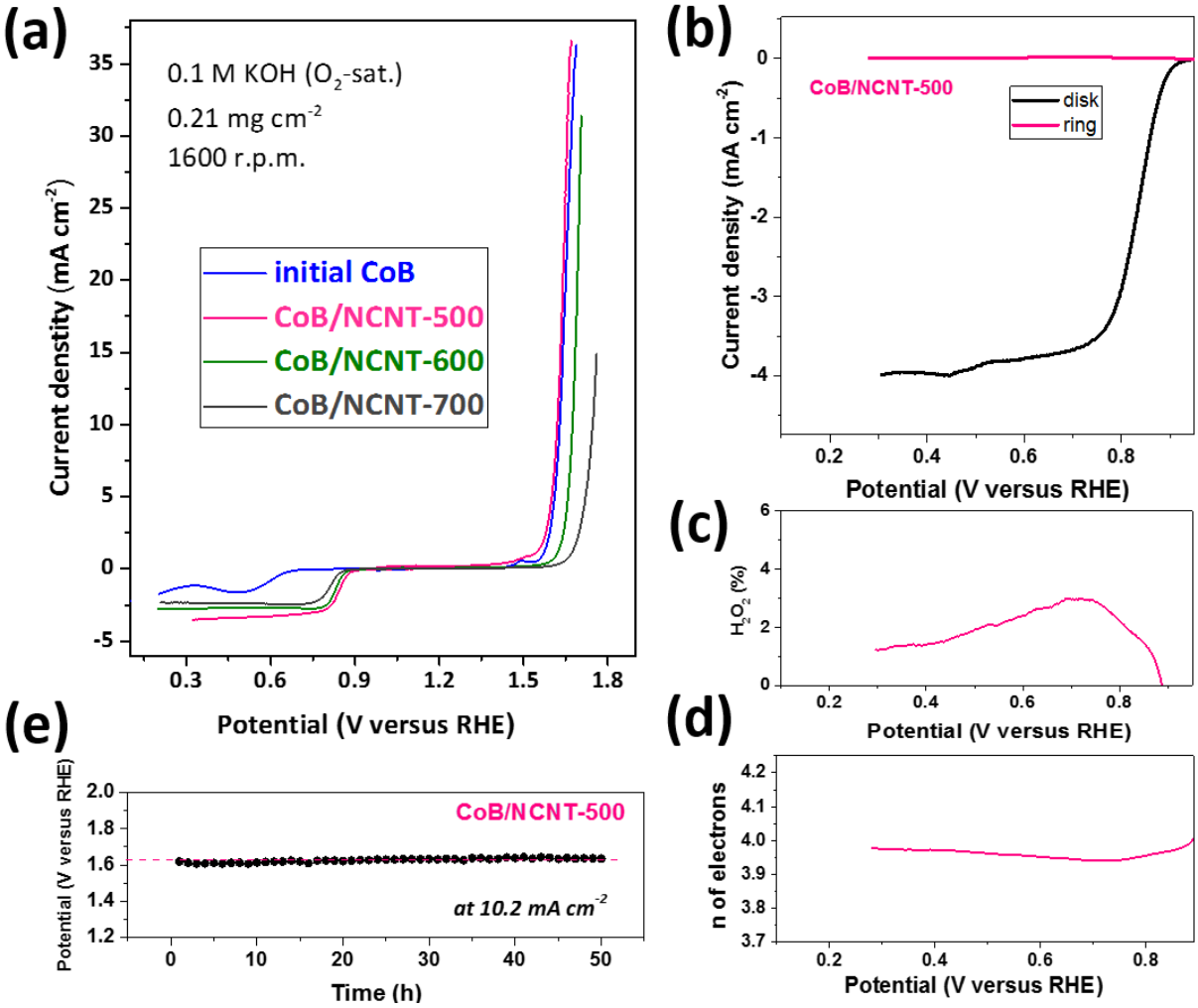

Figure 4. Electrochemical characterization of the CoB/NCNT catalysts prepared at different temperatures. a) Linear sweep voltammograms (iR compensated) recorded in O_2-saturated 0.1 M KOH at 1600 rpm showing the OER and ORR activity of CoB/NCNT prepared at different temperatures compared to the initial cobalt boride. b-d) Rotating ring-disk electrode ORR measurements of CoB/NCNT-500 performed at 1600 rpm, while the ring was held at a constant potential of 1.3 V (vs RHE): ring-disc polarization curves (b), hydrogen peroxide yield (c), number of transferred electrons (d). e) Galvanostatic long-term stability test for OER on CoB/NCNT-500 performed in a flow-through cell at 10.2 mA cm^{-2}.

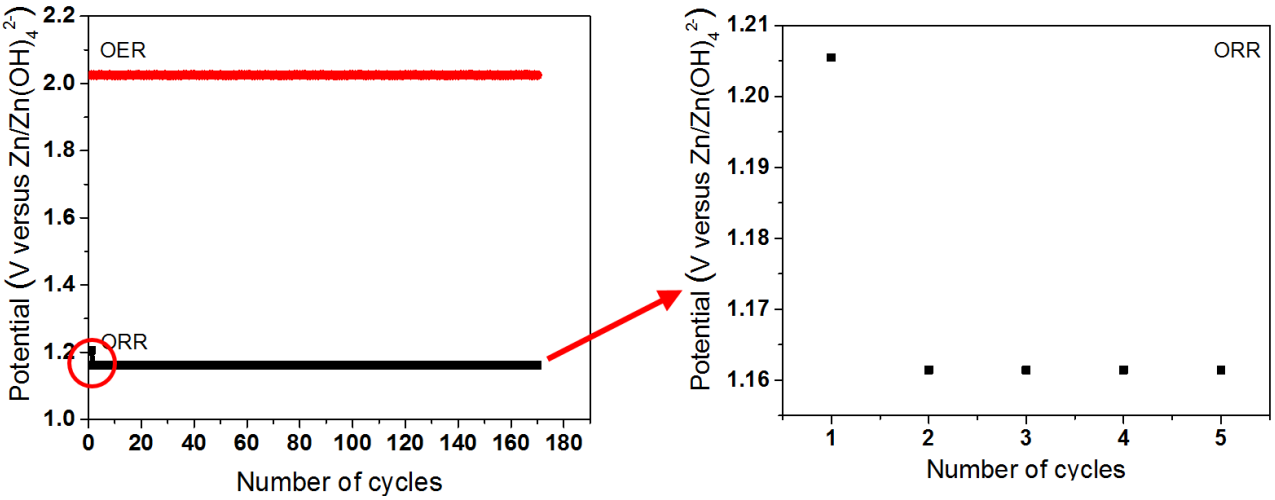

Figure 5. Potential versus number of charge-discharge cycles at ±10 mA cm^{-2} with a 10 min cycle period of the CoB/NCNT-500 spray-coated onto the gas diffusion layer measured in a 3 electrode cell configuration with 6 M KOH as an electrolyte.

Table 1. Elemental composition (wt %) of the CoB/NCNT samples, prepared at different temperatures.

Sample	N	C	H	C/N ratio
CoB/NCNT-500	4.5	59.1	0.4	13.1
CoB/NCNT-600	3.3	83.5	0.4	25.3
CoB/NCNT-700	2.8	87.6	0.5	31.3

Table 2. OER and ORR activity of the CoB/NCNT catalysts expressed as the potential corresponding to -1 mA cm^{-2} (ORR) and +10 mA cm^{-2} (OER) determined from the polarization curves. The bifunctionality parameter $\Delta E_{ORR-OER}$ is the potential difference between the OER and ORR activities at these current densities.

Sample	E_{OER}@+10 mA cm^{-2} / V_{RHE}	E_{ORR}@-1 mA cm^{-2} / V_{RHE}	$\Delta E_{OER-ORR}$ / V_{RHE}
CoB initial	1.62	0.59	1.03
CoB/NCNT-500	**1.60**	**0.87**	**0.73**
CoB/NCNT-600	1.66	0.85	0.81
CoB/NCNT-700	1.73	0.83	0.90

Supporting information

Cobalt boride modified with N-doped carbon nanotubes as high-performance bifunctional oxygen electrocatalyst

Karina Elumeeva, Justus Masa, Danea Medina, Edgar Ventosa, Aziz Genç, Tim Bobrowski, Philipp Weide, Jordi Arbiol, Martin Muhler and Wolfgang Schuhmann**

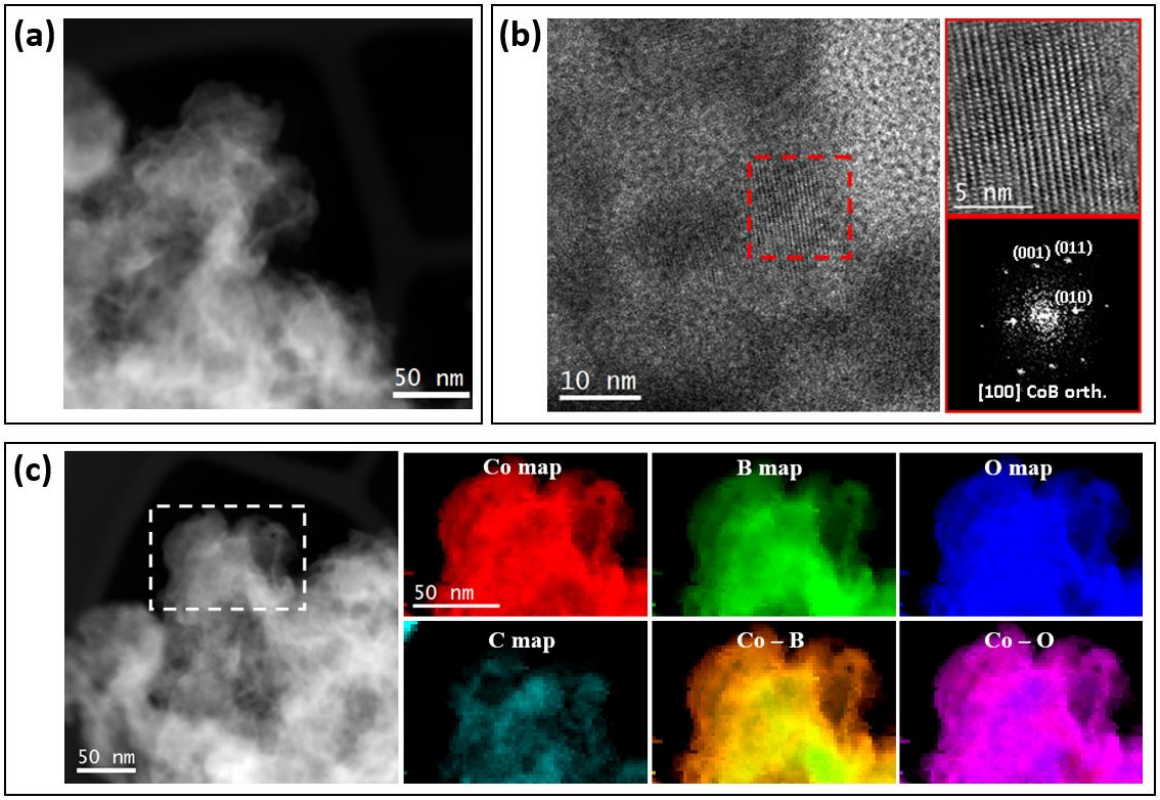

Figure S1. TEM analysis of the initial CoB sample before the electrochemical tests. a) ADF STEM micrograph. b) High-resolution TEM image with an enlarged view of the red squared region showing details of the microstructure and its corresponding power spectrum. c) ADF STEM micrograph and STEM – EELS elemental composition maps of the area indicated with a white rectangle: Co (red), B (green), O (blue), C (turquoise) and N (violet) and their overlay (Co – B, Co – O and C – N). The scale bar is the same for all the compositional maps.

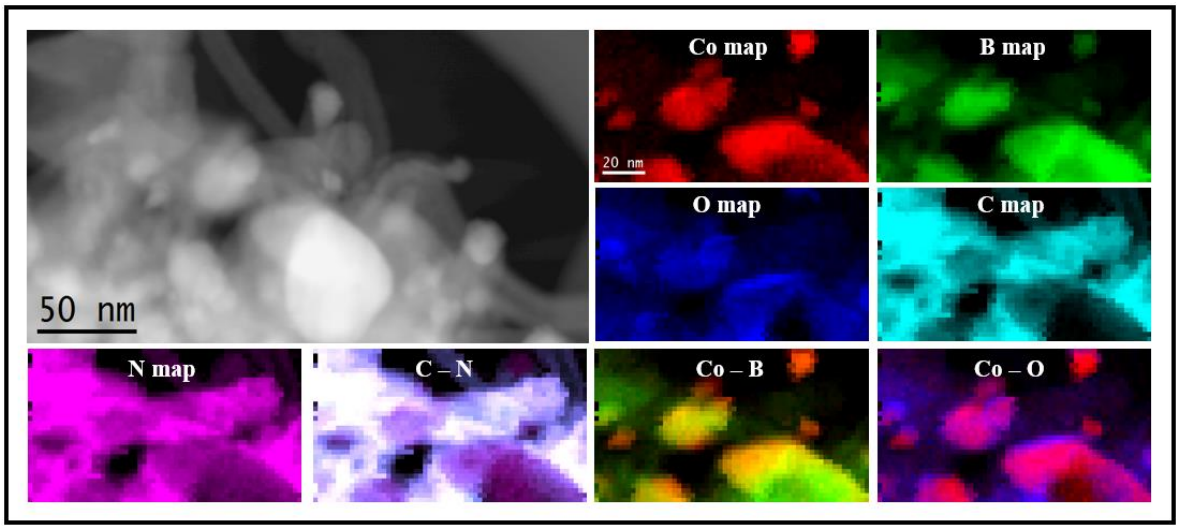

Figure S2. ADF STEM micrograph of CoB/NCNT-500 before electrochemical testing showing an ensemble of nanoparticles and nanotubes, and STEM – EELS elemental composition maps of the area indicated with a white rectangle: Co (red), B (green), O (blue), C (turquoise) and N (violet) and their overlay (Co – B, Co – O and C – N). The scale bar is the same for all the compositional maps.

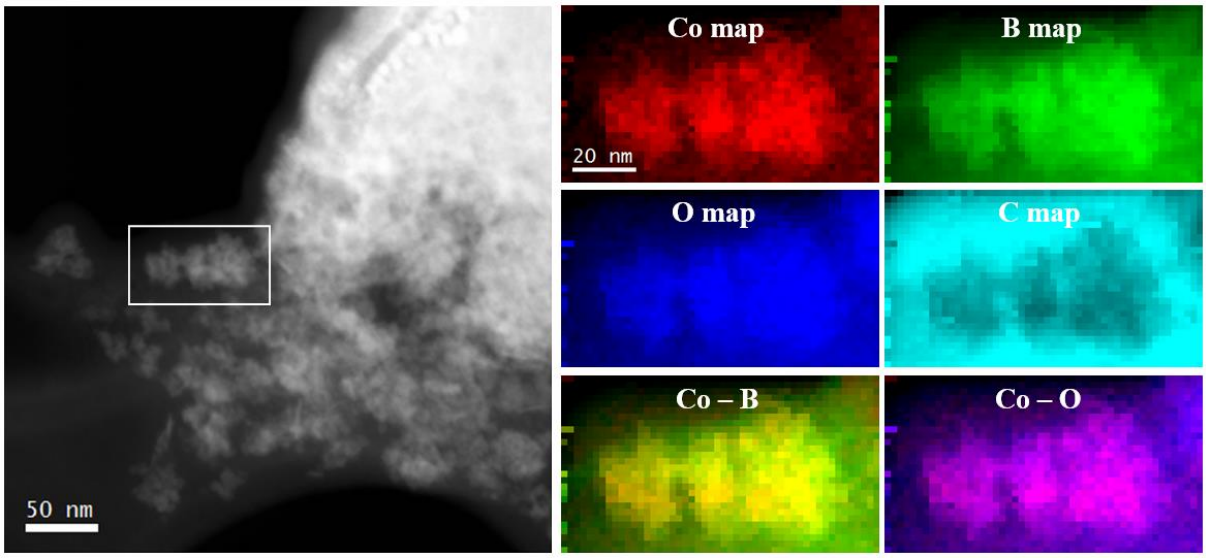

Figure S3. ADF STEM micrograph of CoB/NCNT-500 after electrochemical OER activation showing an ensemble of nanoparticles and nanotubes, and STEM – EELS elemental composition maps of the area indicated with a white rectangle: Co (red), B (green), O (blue), C (turquoise) and N (violet) and their overlay (Co – B, Co – O and C – N). The scale bar is the same for all the compositional maps.

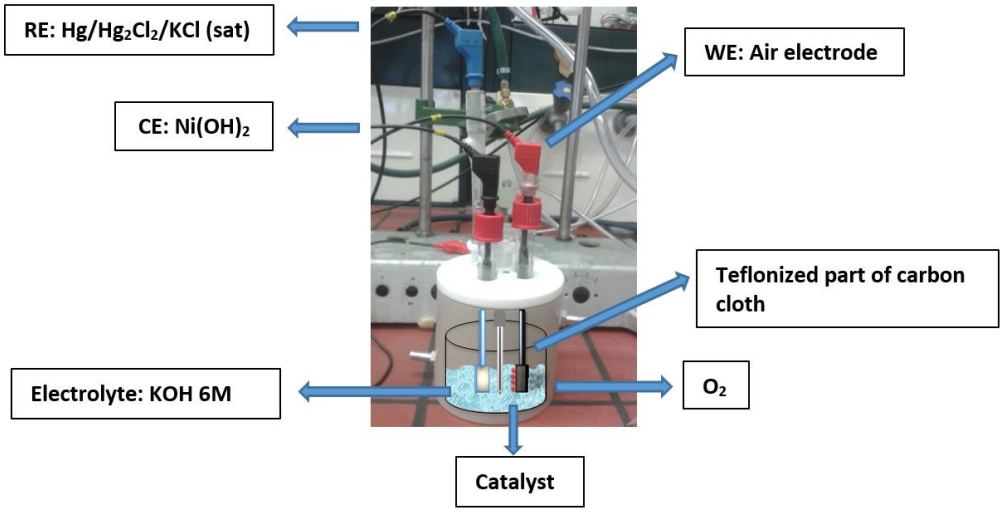

Figure S4. Schematic representation of a home-made electrochemical cell for the charge-discharge stability test in 6 M KOH.

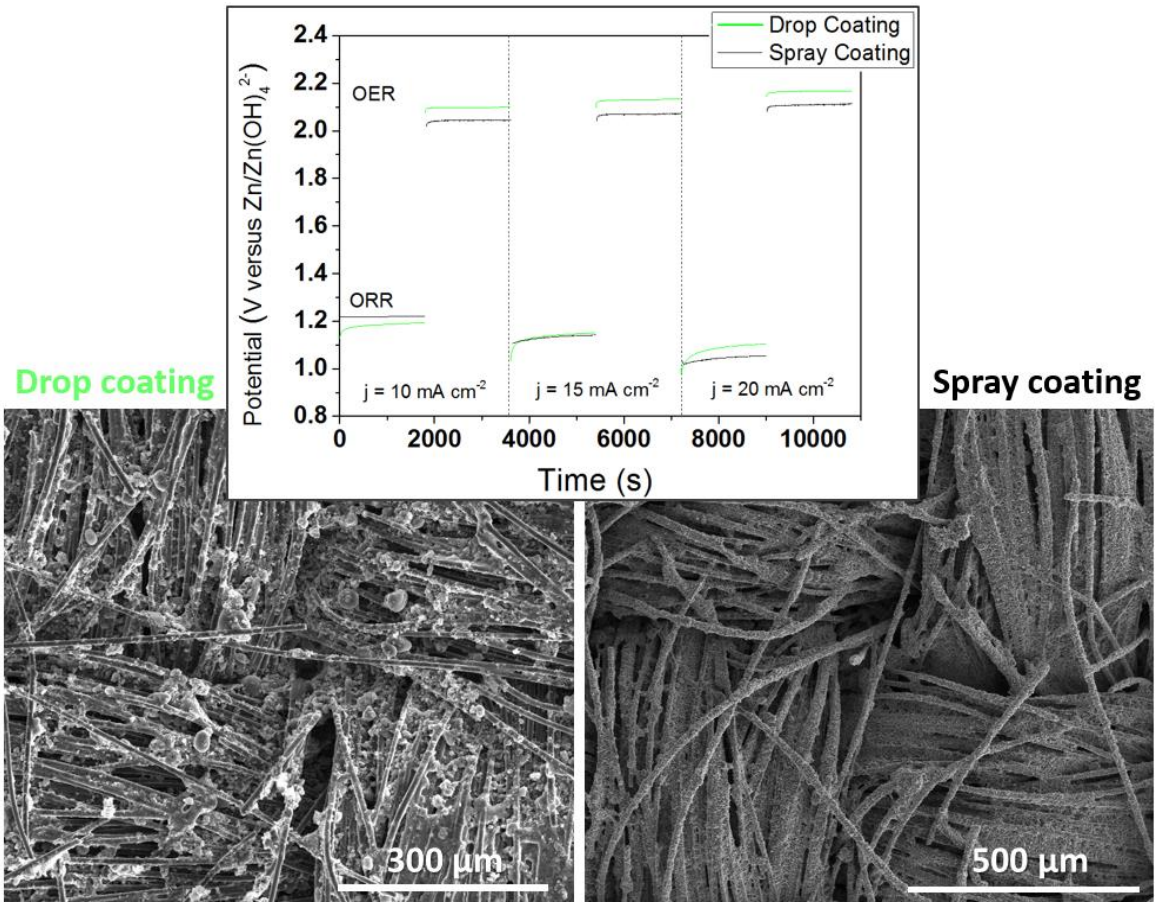

Figure S5. A comparison of the discharge-charge cycling curves with a 1800 s cycle period performed at 10, 15 and 20 mA cm^{-2} (top), and SEM images (bottom) of the air electrodes prepared by drop-coating (left) and spray-coating of CoB/NCNT (right) on carbon cloth teflonized on one side. The deposition was on the non-teflonized side.

Table of contents

A novel bifunctional OER/ORR electrocatalyst synthesized by the direct growth of nitrogen-doped carbon nanotubes on cobalt boride nanoparticles exhibits excellent bifunctional ORR/OER reversibility with a voltage difference between the ORR at -1.0 mA cm^{-2} and the OER at 10 mA cm^{-2} in 0.1 M KOH of only 0.73 V and very promising long-term durability under practical Zn-air battery conditions.